POLITECNICO DI TORINO
Repository ISTITUZIONALE

Strong dopant dependence of electric transport in ion-gated MoS2

Original
Strong dopant dependence of electric transport in ion-gated MoS2 / Piatti, E., Chen, Q., Ye, J.. - In: APPLIED PHYSICS LETTERS. - ISSN 0003-6951. - STAMPA. - 111:1(2017), p. 013106. [10.1063/1.4992477]

Availability:
This version is available at: 11583/2676058 since: 2019-04-19T15:23:18Z

Publisher:
AIP Publishing

Published
DOI:10.1063/1.4992477

Terms of use:

This article is made available under terms and conditions as specified in the corresponding bibliographic description in the repository

Publisher copyright
AIP postprint/Author's Accepted Manuscript e postprint versione editoriale/Version of Record

(Article begins on next page)

27 November 2026

Strong dopant dependence of electric transport in ion-gated MoS_2

Erik Piatti,[1,a)] Qihong Chen,[2] and Jianting Ye[2,b)]
[1]*Department of Applied Science and Technology, Politecnico di Torino, corso Duca degli Abruzzi 24, 10129 TO Torino, Italy*
[2]*Device Physics of Complex Materials, Zernike Institute for Advanced Materials, Nijenborgh 4, 9747 AG Groningen, The Netherlands*

(Received 25 April 2017; accepted 25 June 2017; published online 7 July 2017)

We report modifications of the temperature-dependent transport properties of MoS_2 thin flakes via field-driven ion intercalation in an electric double layer transistor. We find that intercalation with Li^+ ions induces the onset of an inhomogeneous superconducting state. Intercalation with K^+ leads instead to a disorder-induced incipient metal-to-insulator transition. These findings suggest that similar ionic species can provide access to different electronic phases in the same material. *Published by AIP Publishing*. [http://dx.doi.org/10.1063/1.4992477]

Transition metal dichalcogenides are a fascinating class of layered materials, where different orders—such as superconductivity and charge-density waves—compete with each other and give rise to complex phase diagrams reminiscent of those of cuprates and iron pnictides.[1,2] Intercalation by means of a wide range of compounds, both organic and inorganic, is a particularly powerful tool to tune the properties of these materials,[2–4] resulting in superconducting compounds characterized by sharp transition temperatures and well-defined upper critical fields.

In recent years, ionic gating has been utilized to control the transport properties of a wide range of materials, including oxides,[5–11] metal chalcogenides,[12–22] graphene[23–26] and other 2-dimensional materials,[27–29] and even metals.[30–35] Most of these results have been obtained within the electrostatic limit, i.e., by only accumulating ions at the material surface and exploiting the ultrahigh electric field that develops in the electric double layer (EDL).[36] However, ionic gating of layered materials allows for a further degree of freedom in the technique, by exploiting the electric field to intercalate the ions between the van der Waals-bonded layers, thus allowing control over the properties of the entire bulk. This technique has already showcased its possibilities by allowing a robust control of the electronic ground state in TaS_2,[15] $MoTe_2$,[16] WSe_2,[16] and FeSe.[17] These studies mainly focused on the modulation of the bulk carrier density achieved via ion intercalation, without analyzing in detail the effects of different ionic species on the same ion-gated material. In principle, however, the choice of the dopant ion may severely affect the properties of the intercalated phase, leading to ion-specific device behavior and possibly entirely different phase diagrams for the field-induced intercalated state.

Here, we tackle this issue by performing ionic gating experiments on archetypal layered semiconductor MoS_2 using K^+ and Li^+ as dopant ions. MoS_2 is known to undergo a series of insulator-to-metal-to-superconductor phase transitions upon both surface electrostatic carrier accumulation[12] and chemical intercalation with different ionic species.[37,38] We find that, for field-driven intercalation, this is the case only for the smaller Li^+ ion [see the lower panel of Fig. 1(a)]. The larger K^+ ion (upper panel) leads instead to an incipient metal-to-insulator transition for large doping levels due to the introduction of disorder during the intercalation process. This disorder may originate from simple lattice distortions or a more complex coexistence of different incommensurate doped structures, such as those reported in superconducting intercalated TaS_2[39] and Bi_2Se_3.[40] These results demonstrate the critical importance of the specific

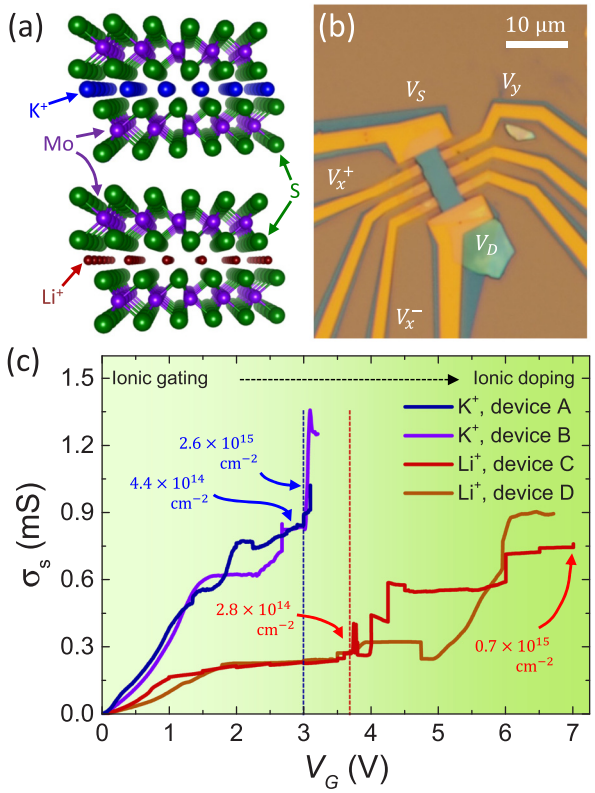

FIG. 1. (a) Ball-and-stick model of the MoS_2 lattice with intercalated K^+ (top panel) and Li^+ (bottom panel) ions.[50] (b) Optical micrograph of a MoS_2 field-effect device before drop-casting the electrolyte. (c) Gate dependence of the sheet conductivity σ_s at $T = 300$ K for both K^+ (devices A and B) and Li^+-based electrolytes (devices C and D). Dashed lines indicate the corresponding threshold voltages for the onset of ion intercalation. The four values of densities correspond to the Hall carrier densities n_H for devices A and C.

a)Electronic mail: erik.piatti@polito.it
b)Electronic mail: j.ye@rug.nl

ionic species and size in ion-gated devices and indicate that different electrolytes can be used to explore different phase diagrams within the same material and device architecture.

We prepared few-layer MoS_2 flakes by micromechanical exfoliation of their bulk crystals (2H polytype, SPI supplies) via the well-known scotch-tape method[41–43] and transferred them on SiO_2(300 nm)/Si substrates. We inspected the flakes with an optical microscope and selected samples with the number of layers between ~5 and 10 by analyzing their reflection contrast.[44] We realized the electrical contacts [Ti(5 nm)/Au(35 nm)] in the Hall bar configuration, together with a co-planar side gate electrode, by standard microfabrication techniques. We patterned and deposited a solid oxide mask (Al_2O_3 thickness ~40 nm) on the metallic leads only to reduce their interaction with the electrolyte during the experiments. Reactive Ion Etching (Ar gas, RF Power 100 W, exposure time 2 min) was used to pattern the flakes into a rectangular shape, in order to achieve a well-defined aspect ratio for sheet resistance measurements. Figure 1(b) presents the optical micrograph of a completed device before drop-casting the polymer electrolyte prepared by dissolving ~25 wt. % of either K^+ or Li^+-based salts in polyethylene glycol (PEG, $M_w \sim 600$). We tested both ClO_4^- and bis(trifluoromethane)sulfonimide ($TFSI^-$)-based salts and observed no significant dependence of the gating efficiency on the anion choice. Both Li^+ and K^+ electrolytes were liquid at room temperature and underwent a glass transition below ~250 K. Transport measurements were performed as a function of the temperature T via the standard lock-in technique in a Quantum Design® Physical Properties Measurement System with minimal exposure to ambient condition.

We accessed the intercalated state in our MoS_2 devices by slowly ($dV_G/dt \sim 2$ mV/s) ramping the gate voltage V_G to a target value at $T = 300$ K and monitoring their conductivity for sharp increases in its value as the signature of the onset of intercalation[15] [see Fig. 1(c)]. However, intercalation allows the ions in the electrolyte to migrate across the entire thickness of the device, and the increase in conductivity may potentially be suppressed by an increase in disorder. Hence, its onset can more reliably be detected as a large increase in the Hall carrier density $n_H = 1/eR_H$ of the device to values comparable with those of a few-nanometer-thick metal ($\sim 10^{15}$ cm^{-2}). These values are one order of magnitude larger than those achievable on MoS_2 upon pure surface accumulation[12,14,16,45] and are thus a reliable signature for the onset of bulk doping.

Thus, when the target V_G was reached, we waited for ~30 min as sufficient time allowing the full relaxation of ion dynamics to improve doping homogeneity. We then cooled the sample to $T \lesssim 240$ K (below the glass transition of the electrolyte) and measured the Hall coefficient R_H by sweeping the magnetic field perpendicular to the surface of the active channel (see supplementary material). At this point, we either performed a full T-dependent characterization of the transport properties of the device by cooling the system down to 2 K or warmed the sample up to 300 K and increased V_G even further. We performed the T-dependent characterization both before (ionic-gating regime) and after (ionic-doping regime) the onset of intercalation on our devices.

Figure 1(c) shows a comparison between the V_G dependence of the sheet conductivity σ_s of four devices, two gated with the $KClO_4$/PEG electrolyte (devices A and B) and the other two with the LiTFSI/PEG electrolyte (devices C and D). While the details of these bias ramps vary between different samples, the same choice of electrolyte results in similar curves across multiple devices. We attribute the random appearance of step features in σ_s to the dynamics of the intercalation process: each step corresponds to a different doping state, and these states are sample-dependent. Moreover, the behavior of K^+- and Li^+-gated devices is clearly different.

We first consider the behavior of a K^+-gated device (device A): in this case, the gate voltage was ramped up to a maximum of +3.1 V, and R_H was measured twice: first at $V_G = +2.8$ V and then at $V_G = +3.1$ V. The corresponding values of n_H show that the carrier density at $V_G = +2.8$ V ($n_H \simeq 4.4 \times 10^{14}$ cm^{-2}) is about six times smaller than the one at $V_G = +3.1$ V ($n_H \simeq 2.6 \times 10^{15}$ cm^{-2}). This strongly suggests that the device is still mainly in the electrostatic accumulation regime at $V_G = +2.8$ V and is instead intercalated at $V_G = +3.1$ V. It is worth noting that this large increase in n_H does not lead to a significant increase in σ_s, indicating that doping with K^+ ions, while inducing carriers, severely reduces the carrier mobility (at $T = 300$ K, $\mu_H \simeq 12 \pm 3$ and 2.5 ± 0.2 cm^2/V s for $V_G = +2.8$ and + 3.1 V, respectively). We can also roughly estimate the nominal doping level x in the K_xMoS_2 stoichiometry at $V_G = +3.1$ V ($K_{0.45}MoS_2$), assuming a uniform distribution of the dopants in all the layers (five for this specific sample). This estimation indicates that the sample at $V_G = +3.1$ V should be completely in the metallic state and in the correct doping range to show superconductivity at low temperature.[37] Inducing larger doping levels in K^+-gated devices by applying gate voltages in excess of $V_G = +3.5$ V always leads to device failure.

Let us focus now on the behavior of a Li^+-gated device (device C). Interestingly, Li^+-gated devices did not show significant signs of intercalation in the same voltage range for which intercalation occurred in the K^+-gated devices. Instead, we observed an electrostatic increase of σ_s with increasing gate voltage up to $V_G \simeq +3.6$ V. Larger voltage values caused a peculiar behavior to emerge, where σ_s appeared to randomly "jump" between high- and low-conductivity states as V_G was increased. This behavior, which may be associated with an unstable incorporation of the Li^+ ions between the MoS_2 layers, continued up to $V_G \simeq +6.1$ V. Even larger gate voltages up to $V_G \simeq +7.0$ V featured a second stable region of monotonically increasing σ_s, which was about 4 times larger than that for $V_G \simeq +3.6$ V. The corresponding values of carrier density, as measured by the Hall effect at $T = 220$ K, were $n_H(+3.6\,V) \simeq 2.8 \times 10^{14}$ cm^{-2} and $n_H(+7.0\,V) \simeq 7.1 \times 10^{14}$ cm^{-2} ($Li_{0.12}MoS_2$), with a Hall mobility $\mu_H \simeq 12 \pm 2$ and 9.2 ± 1.8 cm^2/V s in the two cases, respectively. The significant increase in both σ_s and n_H indicates that the high-conductivity state at $V_G \simeq +7.0$ V may be associated with Li^+ intercalation. The corresponding nominal doping $x \simeq 0.12$ achieved in our sample is still below the onset of superconductivity in chemically intercalated samples, which emerges only for $x \geq 0.4$.[37]

Overall, the following main differences emerge when comparing K^+ and Li^+ intercalation at the same operating temperature ($T = 300$ K): first, the decrease in mobility is much less pronounced in the case of Li^+ doping, indicating a much less prevalent introduction of extra defects in the system; second, while the thickness of the two samples was comparable, the final n_H is significantly smaller in the Li^+-doped one, indicating that K^+ ions are able to more efficiently penetrate between the MoS_2 layers. Furthermore, the onset of K^+ doping requires smaller gate voltages but leads to device degradation for smaller V_G values as well.

We now consider the T-dependent transport properties of our devices down to 2 K in both K^+ and Li^+-doped samples. We characterize our devices first in the electrostatic regime and again after the electric field has driven the ions to intercalate the material.

Figure 2(a) shows the T-dependence of the square resistance R_s of device A, gated with the $KClO_4$/PEG electrolyte, for both ionic gating ($V_G = +2.8$ V, green curve) and ionic doping ($V_G = +3.1$ V, blue curve). When the ions only accumulate at the surface of MoS_2 (low V_G), the device shows a clear metallic behavior, with a smaller low-T value of R_s than that typically displayed by ionic-liquid-gated MoS_2.[12] This is consistent with the larger doping level induced in the sample. Moreover, this suggests that K^+ gating is able to bring MoS_2 beyond the field-induced superconducting dome.[12]

When the ions are able to intercalate the sample, we would also expect a metallic behavior and a further reduction of R_s at low-T. Moreover, given that the doping level $K_{0.45}MoS_2$ determined at 240 K, we would also expect the emergence of a superconducting transition at $T \sim 6$ K.[38] However, the T-dependence of R_s in the intercalated state does not show any of these features. Instead, it shows a clear non-monotonic behavior and two regions where R_s decreases for increasing T: one for $T \gtrsim 150$ K and the other for $T \lesssim 20$ K. The second one, the low-temperature upturn, is insensitive to the applied magnetic field, ruling out a possible contribution from weak localization. For intermediate temperatures, R_s increases as $e^{-A/T}$, $A \simeq 107$ K [see Fig. 2(b)]. This type of behavior is reminiscent of a two-dimensional system very close to a metal-to-insulator transition.[46,47]

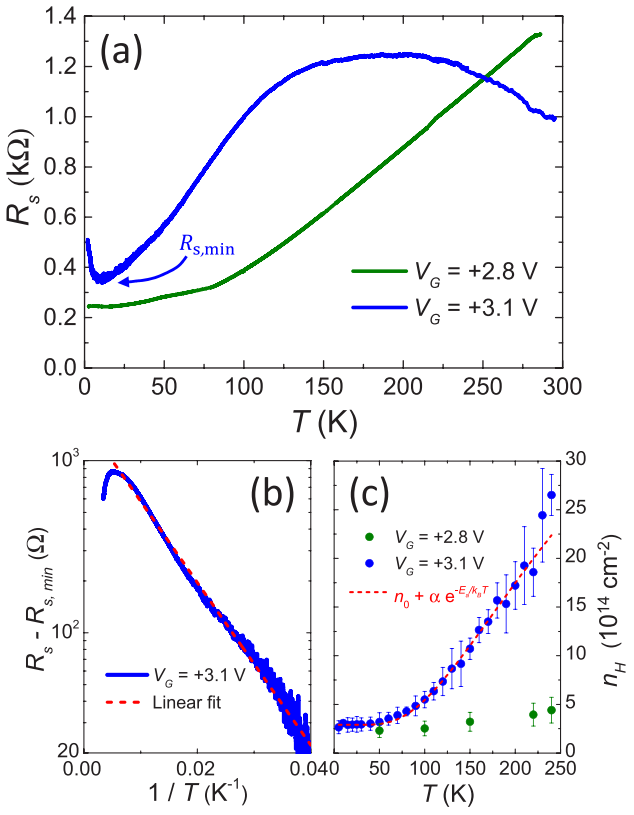

FIG. 2. T-dependent transport properties of K^+-gated MoS_2. (a) R_s vs. T for K^+ accumulation (solid green line) and intercalation (solid blue line). (b) $R_s - R_{s,min}$ as a function of T^{-1} in the intercalated state. The dashed red line is a linear fit to the curve to highlight its exponential dependence. (c) n_H vs. T corresponding to the curves of (a). The dashed red line is a fit to the thermally activated behavior.

These results indicate the peculiar condition of a system being close to becoming an insulator, while at the same time presenting a metal-like density of charge carriers at high T. Thus, we investigated whether n_H was metallic at low-T as well. Figure 2(c) shows the T-dependence of n_H obtained from Hall effect measurements. It is apparent that n_H in the bulk doped state (blue dots) strongly decreases at the reduction of T. Indeed, the T-dependence of n_H can be separated into two contributions: a relatively small constant value $n_0 \simeq 2.9 \times 10^{14}$ cm^{-2} and an Arrhenius-like term $n(T) \propto e^{-E_a/k_BT}$, where $E_a \simeq 0.03$ eV is an activation energy and k_B is the Boltzmann constant. For comparison, the carrier density induced by surface ionic gating (green dots) is much less T-dependent, while at the same time reaching nearly the same low-T value. The resulting low-T mobilities are $\mu_H \simeq 110 \pm 33$ and 50 ± 12 cm^2/V s for K^+ accumulation and intercalation, respectively. Thus, it is natural to assume that the quasi-constant term arises from ionic gating at the sample surface, while the thermally activated one is associated with bulk ion doping.

We thus suggest that the electrochemically intercalated K^+ ions are behaving as thermally activated electron donors and reside in shallow trap states in the bulk MoS_2 energy gap: the material thus behaves more like a highly doped but highly defective semiconductor with a field-induced metallic channel at its surface, instead of showing a proper metallic character across its entire thickness. Moreover, this very defective character of the K^+-doped regime is able to account for both the sharp reduction in carrier mobility and the emergence of an Anderson-like localization regime at low T. A disorder-induced metal-to-insulator transition was recently reported in ion-gated monolayer ReS_2[18] but not in any ion-gated multilayer transition metal dichalcogenide.

In Fig. 3(a) instead, we present the R_s vs. T behavior of device C, gated with the LiTFSI/PEG electrolyte. The yellow and red curves refer to Li^+-gating ($V_G = +3.6$ V) and doping ($V_G = +7.0$ V), respectively. The inset shows the corresponding T-dependence of their sheet carrier density n_H as measured by the Hall effect. Unlike the K^+ ion, the Li^+ ion allows the system to retain a full metallic behavior also in the bulk doping regime, without evidences of non-monotonicity or low-T upturns. The T-dependence of n_H is also less pronounced, being nearly constant for $T \lesssim 150$ K in the case of ionic gating and losing less than half of its high-T value in the case of ionic doping. Indeed, the low-T carrier density in the Li^+-doped state, $n_H \simeq 3.9 \times 10^{14}$ cm^{-2}, was significantly larger than the one for K^+ doping, even though its nominal doping level x was nearly 3 times smaller. This

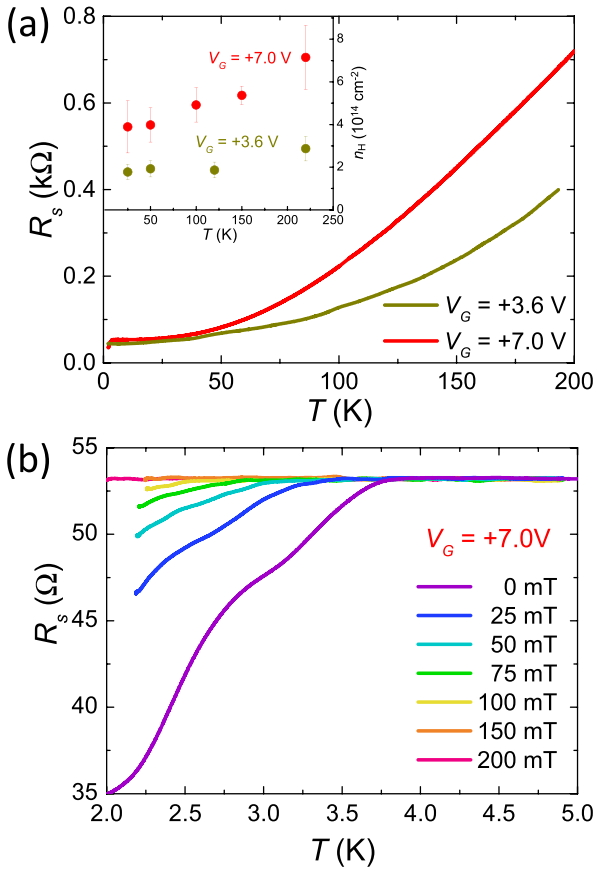

FIG. 3. T-dependent transport properties of Li^+-gated MoS_2. (a) R_s vs. T for Li^+ accumulation (solid yellow line) and intercalation (solid red line). The inset shows the corresponding carrier densities n_H. (b) R_s vs. T in the intercalated state below 5 K for different values of the applied magnetic field.

indicates that, in the case of Li^+ doping, the smaller density of defects acting as shallow trap states allows for a higher fraction of charge carriers to participate in conduction at low T. This reduced density of defects is also apparent in the low-T mobilities $\mu_H \simeq 800 \pm 160$ and $300 \pm 94\,\mathrm{cm}^2/\mathrm{V\,s}$ for Li^+ gating and doping, respectively, several times larger than the ones we observed in the case of the K^+ ion.

The most likely explanation of these results is that the size of the K^+ ion is too large to be able to intercalate the MoS_2 lattice without introducing significant distortions and defects in its entire volume. These defects would then act as shallow trap states, capturing most of the transferred electrons at low T and suppressing the metallic behavior except in the thin layer at the surface due to electrostatic accumulation. We note that a similar disruptive effect of large intercalating species was also observed in ion-gated TaS_2, where it leads to abrupt device failure.[15] It is interesting then to consider why the larger K^+ ion shows an enhanced doping efficiency with respect to the smaller Li^+. We suggest that this behavior may arise from the lattice distortions introduced during the intercalation process allowing the K^+ ions still dissolved in the electrolyte to diffuse more easily through the damaged regions. On the other hand, the lattice remains relatively unaffected during the intercalation by the smaller Li^+ ions, thus requiring larger driving voltages to intercalate the bulk of the sample. However, further investigations—such as disorder studies by means of x-ray diffraction—are needed to clarify this issue.

Further evidence of the importance of dopant size on the behavior of ion-gated devices lies in the fact that we were able to observe a clear downturn in the R_s vs. T curve in the Li^+-doped state below 4 K. Figure 3(b) shows its response to the application of a magnetic field perpendicular to the active channel of the device. While the downturn never reaches a zero-resistance state, its suppression by a magnetic field is precisely the behavior expected from a superconducting transition. We point out that while the nominal doping level at $V_G = +7.0$ V was estimated to be $Li_{0.12}MoS_2$, the onset temperature of the downturn ($T_c^{on} \simeq 3.7$ K) agrees well with that of chemically doped Li_xMoS_2 for $x \geq 0.4$.[38] Moreover, superconductivity does not appear in chemically doped Li_xMoS_2 for $x \leq 0.4$.[38] Since we observe a superconducting onset, the doping level in the intercalated state must be strongly inhomogeneous. This is supported by the behavior of the superconducting transition: the R_s vs. T profile is not the sharp drop associated with homogeneous bulk superconductivity. Instead, the transition is broad and strongly suggestive of multiple phases. This kind of behavior is typical of granular superconductors: in the Li^+-doped state, only a handful of regions are able to reach a doping level large enough to induce a superconducting state, while most of the active channel remains metallic and prevents the realization of homogeneous 3D superconductivity. The slowly vanishing resistance tail is due to Josephson tunneling between the superconducting regions (weak-link superconductivity).[48,49]

In conclusion, we employed polymer electrolyte gating to intercalate MoS_2 thin flakes with different ionic species. We unveiled the critical role of ionic size in the determination of the electric transport properties of the intercalated devices. The larger K^+ ions were found to strongly damage the MoS_2 lattice leading to an incipient metal-to-insulator transition at high doping levels. The smaller Li^+ ions preserved the metallic character of the devices and allowed the emergence of an inhomogeneous bulk superconducting phase. These findings highlight the critical role of the ionic medium in electrochemically gated devices, for both electrostatic carrier accumulation and field-driven ion intercalation.

See supplementary material for further details on the measurement setup, Hall effect measurements, and optical characterization of the intercalation process.

We thank R. S. Gonnelli for perusing the manuscript and useful scientific discussions. We acknowledge funding from the European Research Council (Consolidator Grant No. 648855 Ig-QPD).

[1]R. A. Klemm, *Layered Superconductors* (Oxford University Press, Oxford, UK, New York, NY, 2012), Vol. 1.
[2]R. A. Klemm, Physica C **514**, 86 (2015).
[3]A. Lerf and R. Schöllhorn, Inorg. Chem. **16**, 2950 (1977).
[4]Y. Onuki, S. Yamanaka, R. Inada, M. Kido, and S. Tanuma, Synth. Met. **5**, 245 (1983).
[5]K. Ueno, S. Nakamura, H. Shimotani, A. Ohtomo, N. Kimura, T. Nojima, H. Aoki, Y. Iwasa, and M. Kawasaki, Nat. Mater. **7**, 855–858 (2008).
[6]K. Ueno, S. Nakamura, H. Shimotani, H. T. Yuan, N. Kimura, T. Nojima, H. Aoki, Y. Iwasa, and M. Kawasaki, Nat. Nanotechnol. **6**, 408 (2011).

[7]A. T. Bollinger, G. Dubuis, J. Yoon, D. Pavuna, J. Misewich, and I. Božović, Nature **472**, 458 (2011).
[8]X. Leng, J. Garcia-Barriocanal, S. Bose, Y. Lee, and A. M. Goldman, Phys. Rev. Lett. **107**, 027001 (2011).
[9]X. Leng, J. Garcia-Barriocanal, B. Yang, Y. Lee, J. Kinney, and A. M. Goldman, Phys. Rev. Lett. **108**, 067004 (2012).
[10]J. Jeong, N. B. Aetukuri, T. Graf, T. D. Schladt, M. G. Samant, and S. S. P. Parkin, Science **339**, 1402 (2013).
[11]K. Jin, W. Hu, B. Zhu, J. Yuan, Y. Sun, T. Xiang, M. S. Fuhrer, I. Takeuchi, and R. L. Greene, Sci. Rep. **6**, 26642 (2016).
[12]J. T. Ye, Y. J. Zhang, R. Akashi, M. S. Bahramy, R. Arita, and Y. Iwasa, Science **338**, 1193 (2012).
[13]S. H. Jo, D. Costanzo, H. Berger, and A. F. Morpurgo, Nano Lett. **15**(2), 1197 (2015).
[14]D. Costanzo, S. Jo, H. Berger, and A. F. Morpurgo, Nat. Nanotechnol. **11**, 339 (2016).
[15]Y. Yu, F. Yang, X. F. Lu, Y. J. Yan, Y.-H. Cho, L. Ma, X. Niu, S. Kim, Y.-W. Son, D. Feng, S. Li, S.-W. Cheong, X. H. Chen, and Y. Zhang, Nat. Nanotechnol. **10**, 270 (2015).
[16]W. Shi, J. T. Ye, Y. Zhang, R. Suzuki, M. Yoshida, J. Miyazaki, N. Inoue, Y. Saito, and Y. Iwasa, Sci. Rep. **5**, 12534 (2015).
[17]B. Lei, N. Z. Wang, C. Shang, F. B. Meng, L. K. Ma, X. G. Luo, T. Wu, Z. Sun, Y. Wang, Z. Jiang, B. H. Mao, Z. Liu, Y. J. Yu, Y. B. Zhang, and X. H. Chen, Phys. Rev. B **95**, 020503(R) (2017).
[18]D. Ovchinnikov, F. Gargiulo, A. Allain, D. J. Pasquier, D. Dumcenco, C. H. Ho, O. V. Yazyev, and A. Kis, Nat. Commun. **7**, 12391 (2016).
[19]L. J. Li, E. C. T. O'Farrell, K. P. Loh, G. Eda, B. Özyilmaz, and A. H. Castro Neto, Nature **529**, 185 (2016).
[20]X. X. Xi, H. Berger, L. Forró, J. Shan, and K. F. Mak, Phys. Rev. Lett. **117**, 106801 (2016).
[21]J. Shiogai, Y. Ito, T. Mitsuhashi, T. Nojima, and A. Tsukazaki, Nat. Phys. **12**, 42 (2016).
[22]B. Lei, J. H. Cui, Z. J. Xiang, C. Shang, N. Z. Wang, G. J. Ye, X. G. Luo, T. Wu, Z. Sun, and X. H. Chen, Phys. Rev. Lett. **116**, 077002 (2016).
[23]D. K. Efetov and P. Kim, Phys. Rev. Lett. **105**, 256805 (2010).
[24]J. T. Ye, M. F. Craciun, M. Koshino, S. Russo, S. Inoue, H. T. Yuan, H. Shimotani, A. F. Morpurgo, and Y. Iwasa, Proc. Natl. Acad. Sci. U.S.A. **108**(32), 13002 (2011).
[25]R. S. Gonnelli, F. Paolucci, E. Piatti, K. Sharda, A. Sola, M. Tortello, J. R. Nair, C. Gerbaldi, M. Bruna, and S. Borini, Sci. Rep. **5**, 9554 (2015).
[26]E. Piatti, S. Galasso, M. Tortello, J. R. Nair, C. Gerbaldi, M. Bruna, S. Borini, D. Daghero, and R. S. Gonnelli, Appl. Surf. Sci. **395**, 37 (2017).
[27]J. T. Ye, S. Inoue, K. Kobayashi, Y. Kasahara, H. T. Yuan, H. Shimotani, and Y. Iwasa, Nat. Mater. **9**, 125 (2010).
[28]Y. Saito, Y. Kasahara, J. T. Ye, Y. Iwasa, and T. Nojima, Science **350**(6259), 409 (2015).
[29]Y. Saito and Y. Iwasa, ACS Nano **9**, 3192 (2015).
[30]D. Daghero, F. Paolucci, A. Sola, M. Tortello, G. A. Ummarino, M. Agosto, R. S. Gonnelli, J. R. Nair, and C. Gerbaldi, Phys. Rev. Lett. **108**, 066807 (2012).
[31]H. Nakayama, J. T. Ye, T. Ohtani, Y. Fujikawa, K. Ando, Y. Iwasa, and E. Saitoh, Appl. Phys. Express **5**, 023002 (2012).
[32]M. Tortello, A. Sola, K. Sharda, F. Paolucci, J. R. Nair, C. Gerbaldi, D. Daghero, and R. S. Gonnelli, Appl. Surf. Sci. **269**, 17 (2013).
[33]J. Choi, R. Pradheesh, H. Kim, H. Im, Y. Chong, and D. H. Chae, Appl. Phys. Lett. **105**, 012601 (2014).
[34]E. Piatti, A. Sola, D. Daghero, G. A. Ummarino, F. Laviano, J. R. Nair, C. Gerbaldi, R. Cristiano, A. Casaburi, and R. S. Gonnelli, J. Supercond. Novel Magn. **29**, 587–591 (2016).
[35]E. Piatti, D. Daghero, G. A. Ummarino, F. Laviano, J. R. Nair, R. Cristiano, A. Casaburi, C. Portesi, A. Sola, and R. S. Gonnelli, Phys. Rev. B **95**, 140501(R) (2017).
[36]K. Ueno, H. Shimotani, H. Yuan, J. T. Ye, M. Kawasaki, and Y. Iwasa, J. Phys. Soc. Jpn. **83**, 032001 (2014).
[37]J. A. Woollam and R. B. Somoano, Mater. Sci. Eng. **31**, 289 (1977).
[38]R. B. Somoano, V. Hadek, and A. Rembaum, J. Chem. Phys. **58**, 697 (1973).
[39]Y. Kashihara and H. Yoshioka, J. Phys. Soc. Jpn. **50**, 2084 (1981).
[40]Y. S. Hor, A. J. Williams, J. G. Checkelsky, P. Roushan, J. Seo, Q. Xu, H. W. Zandbergen, A. Yazdani, N. P. Ong, and R. J. Cava, Phys. Rev. Lett. **104**, 057001 (2010).
[41]R. F. Frindt, Phys. Rev. Lett. **28**, 299 (1972).
[42]F. Bonaccorso, A. Lombardo, T. Hasan, Z. P. Sun, L. Colombo, and A. C. Ferrari, Mater. Today **15**, 564 (2012).
[43]K. S. Novoselov, D. Jiang, F. Schedin, T. J. Booth, V. V. Khotkevich, S. V. Morozov, and A. K. Geim, Proc. Natl. Acad. Sci. USA **102**, 10451 (2005).
[44]H. Li, J. Wu, X. Huang, G. Lu, J. Yang, X. Lu, Q. Xiong, and H. Zhang, ACS Nano **7**, 10344 (2013).
[45]J. Biscaras, Z. Chen, A. Paradisi, and A. Shukla, Nat. Commun. **6**, 8826 (2015).
[46]Y. Hanein, U. Meirav, D. Shahar, C. C. Li, D. C. Tsui, and H. Shtrikman, Phys. Rev. Lett. **80**, 1288 (1998).
[47]Y. Meir, Phys. Rev. Lett. **83**, 3506 (1999).
[48]K. K. Likharev, Rev. Mod. Phys. **51**, 101 (1979).
[49]J. H. Claassen, Appl. Phys. Lett. **36**, 771 (1980).
[50]K. Momma and F. Izumi, J. Appl. Crystallogr. **44**, 1272 (2011).